

---

# Representation mitosis in wide neural networks

---

Diego Doimo\*   Aldo Glielmo   Sebastian Goldt   Alessandro Laio

International School for Advanced Studies (SISSA)  
Trieste, Italy

## Abstract

Deep neural networks (DNNs) defy the classical bias-variance trade-off: adding parameters to a DNN that exactly interpolates its training data will typically improve its generalisation performance. Explaining the mechanism behind the benefit of such over-parameterisation is an outstanding challenge for deep learning theory. Here, we study the last layer representation of various deep architectures such as Wide-ResNets for image classification and find evidence for an underlying mechanism that we call *representation mitosis*: if the last hidden representation is wide enough, its neurons tend to split into groups which carry identical information, and differ from each other only by a statistically independent noise. Like in a mitosis process, the number of such groups, or “clones”, increases linearly with the width of the layer, but only if the width is above a critical value. We show that a key ingredient to activate mitosis is continuing the training process until the training error is zero. Finally, we show that in one of the learning tasks we considered, a wide model with several automatically developed clones performs significantly better than a deep ensemble based on architectures in which the last layer has the same size as the clones.

## 1 Introduction

Deep neural networks (DNN) have enough parameters to easily fit all of their training data, even with random labels [1, 2]. In defiance of the classical bias-variance trade-off, the performance of these *interpolating classifiers* continuously improves as the number of parameters increases well beyond the number of training samples [3–6]. Despite recent progress in describing the implicit bias of stochastic gradient descent towards “good” minima [7–12], and the detailed analysis of solvable models of learning [13–24], the mechanisms underlying this “benign overfitting” [25] in DNNs remain partially unclear, especially since “bad” local minima exist in the optimisation landscape of DNNs [26].

In this paper, we investigate a mechanism that gives rise to benign overfitting in wide, deep neural networks which we call *representation mitosis*. The full *representation* of an input in a trained DNN is given by the last hidden layer of neurons, before the final fully-connected linear layer (Fig. 1 A). Our key observation is that randomly chosen subsets, or “chunks”, of neurons of the full representation classify the inputs with almost the same accuracy as the full representation, without any additional fine-tuning of the last-layer weights. As the network grows wider, its final representation splits into more and more statistically independent chunks, in a process akin to *mitosis* in cell biology [27]. For wide networks, each chunk with a sufficiently large number of neurons can be considered a clone: its representation of the input differs from that of the full layer only by some small, uncorrelated noise. The DNN accuracy then improves with the width of the network because the network implicitly averages over an increasing number of clones in its representations to make its prediction.

---

\*ddoimo@sissa.it

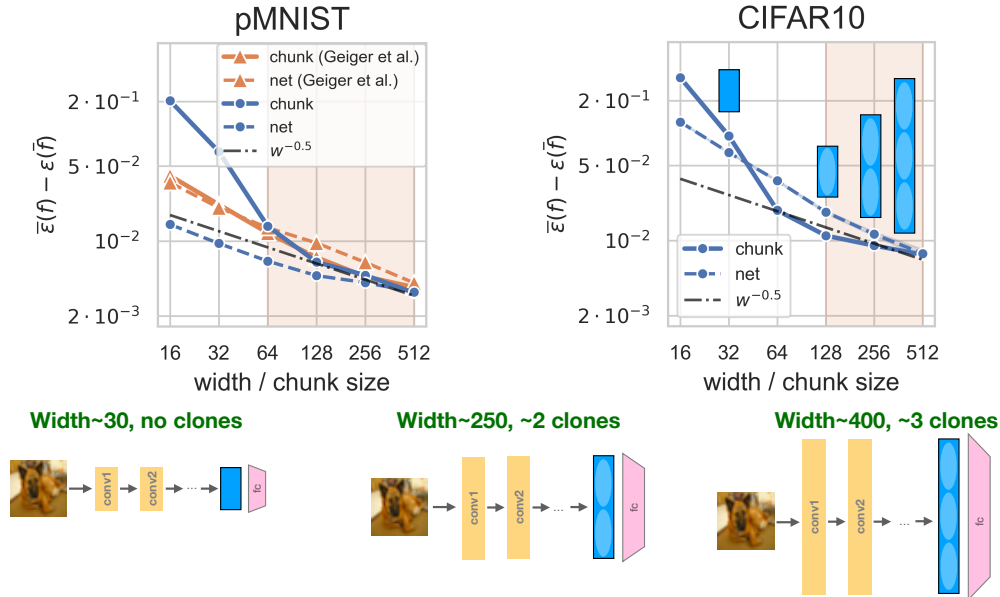


Figure 1: **Representation mitosis as a mechanism for neural scaling laws.** We study the final representations of deep neural networks, which are the activities of the neurons in the last hidden layer before the final fully-connected layer. As we increase the width of the final representation, the average test error  $\bar{\varepsilon}(f)$  of fully-connected neural networks trained on pMNIST (left) and of Wide-ResNets architectures [28] trained on CIFAR10 (right) approaches an asymptotic plateau value  $\varepsilon(\bar{f})$  following a power-law  $\sim \text{width}^{-1/2}$ . Randomly chosen subsets of the neurons in the last layer of the widest networks, that we call “chunks”, perform as well as networks of the same size after some critical width. Here we analyse a mechanism that explains this behaviour: the last layer of overparametrized wide networks can be considered a union of smaller identical representations, which we call “clones”, that differ from each other only by a small and uncorrelated noise. The chunk sizes for which this process happens is highlighted in transparent orange.

We summarise our main observation in Fig. 1. We considered two different learning tasks: the classification of the parity of MNIST digits [29] with a fully-connected network following the protocol of Geiger et al. [24], and the ten-class classification of CIFAR10 [30] with a family of Wide-ResNet-28 [28] networks. In both cases, the prediction of the network is computed from the final hidden representation by applying a linear transformation. As we increase the width of the network, and hence the width of its final representation, the performance improves continuously: the average classification error  $\bar{\varepsilon}(f)$  of 20 networks approaches the performance of an ensemble of networks  $\varepsilon(\bar{f})$  as the width increases, where  $f$  is the function represented by a single network, see Fig. 1.

The key observation that triggered our investigation is that the test accuracy of a model obtained by selecting a chunk of  $w$  neurons from the final representation of the widest network achieves a classification accuracy that is *approximately equal* to that of a full network in which the last layer has the same width  $w$  (orange lines). Crucially, the accuracy of these networks is computed without any re-training after the selection of the activations. We note that the error scales approximately as the inverse square root of the chunk size  $w$ . This scaling suggests the mitosis mechanism described above and sketched at the bottom of the figure: as the width of the network increases, the final representation tends to split into clones which provide statistically independent measures of the same data manifold. The wider the representation, the more clones appear, and the higher the prediction accuracy of the network, as would be expected for an average of independent measures of the same quantity. This mechanism was indeed shown to be optimal in a series of theoretical works for two-layer neural networks [31–36]: the global minima for these shallow networks are characterised by individual neurons developing redundant representations of the important features of the data.

This paper attempts to provide a quantitative analysis of representation mitosis. Our main findings can be summarised as follows:

- A chunk of size  $w$  of the last layer of a wide neural network and the full layer of a network of the same size have very similar statistical properties.
- When the random chunks are large enough to fit the training set they can be linearly mapped one to another with an error which can be described as uncorrelated random noise. In this regime they behave as ‘clones’;
- The clones are a result of persistent training of a well regularised model. Carrying on training until a model has reached zero training error triggers the creation of redundancies in the final representation (clones) that can be helpful for generalisation, rather than hurting it due to overfitting;
- While in pMNIST the accuracy of a model obtained by taking the average over  $n$  independent networks of width  $w$  is practically equivalent to the accuracy of a single model of width  $n \cdot w$ , in CIFAR10, for a given memory requirement, taking the average of the clones generated by a wide network allows reaching a significantly higher accuracy than taking an ensemble average of independently trained networks;
- Deep convolutional neural networks can converge to solutions with the redundant representations predicted by mean-field theories for two-layer neural networks.

## 1.1 Further related work

**Deep ensembles** We found that DNNs create an ensemble of clones in their final representation. It is well known that ensembles of predictors, trained from different initial conditions on the same task, can beat single models in classification and regression (see Ref. [37] for a review). However, the high cost of training deep neural network models often make ensemble approaches prohibitively expensive. Lakshminarayanan et al. [38] proposed deep ensembles to offer uncertainty estimates of deep learning predictions. Littwin et al. [39] introduced “collegial ensembles”, where multiple independent models are trained as a single model in the neural tangent kernel (NTK) [40] regime. Recent theoretical work on random features [21–23] does indeed suggest that ensembling and over-parameterisation are two sides of the same coin in the lazy regime of neural networks [40, 41], where the weights of the networks’ hidden layers don’t move much during training. In this paper, instead we focus on networks in the feature learning regime where weights move significantly [41].

**Neural scaling laws** Capturing the asymptotic performance of neural network via scaling laws is another active research area. In the context of deep learning, Refs. [42–44] experimentally explored the scaling of the generalisation error of deep networks with the number of parameters/data points across architectures and application domains for supervised learning, while Ref. [45] identified empirical scaling laws in generative models. Geiger et al. [24] found that that the generalisation error of fully-connected networks trained on the pMNIST task we also consider scales with the number of parameters. In a similar vein, the authors of Refs. [46] empirically demonstrated the existence of four scaling regimes and described them theoretically in the setting of random features. Ref. [47] relate the exponent of such scaling laws to the dimension of the data manifold.

## 2 Methods

**pMNIST experiments.** We train a fully-connected network to classify the parity of the MNIST digits (pMNIST) following the protocol of Geiger et al. [24]. In short, MNIST digits are projected on the first ten principal components, which are then used as inputs of a five layer fully-connected network (FC5). The four hidden representations have all the same width  $w$  and the output is a real number whose sign is the predictor of the parity of the input digit. In a first experiment the network is fitted like in Ref. [24], without any additional explicit regularizer, minimising the squared hinge loss with full batch gradient descent using Adam optimiser on 10000 digits, until the training loss reaches zero. We run a second test adding batch normalisation and training the same network for 5000 epochs with SGD with momentum of 0.9 using a cosine annealing learning rate scheduler and a batch size of 256. We tuned the learning rate and amount of weight decay using grid search, and report results for learning rate  $10^{-3}$  and weight decay  $10^{-2}$ . With the only exception of the orange profiles in Fig. 1 the results of this work are based on this second setting.

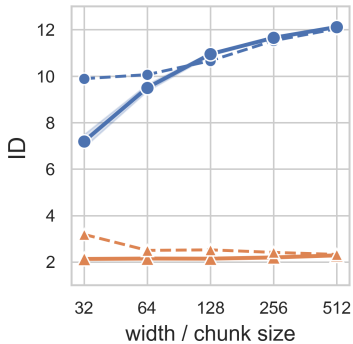


Figure 2: **Intrinsic dimension of representation.** Dashed lines: the ID of the representation of the last layer as a function of its width. Orange: the pMNIST dataset; blue: the CIFAR10 dataset. Solid lines: the ID of chunks of the representation of the last layer (512 neurons in both datasets) as a function of the chunk size. In both datasets the ID of a chunk is very similar to the ID of the full representation of equal width, provided that the width is sufficiently large.

**CIFAR10 experiments.** We then analyse a family of Wide-ResNet-28 [28] (WR28) trained on CIFAR10. The WR28 models are trained for 200 epochs with stochastic gradient descent following standard practice to set the relevant hyper-parameters: batch size = 128, momentum = 0.9, weight decay =  $5 \cdot 10^{-4}$ , and cosine annealing scheduler starting with a learning rate of 0.1. We mildly augmented the training set performing horizontal flips and random cropping the images padded with four pixels on each side. We verified that all our models achieve a performance in agreement with the state of the art with these settings [28, 48, 49]. All our experiments were run on a single GPU GeForce GTX TITAN X.

**Subsampling the final representations.** In the next sections we measure the width of the last hidden representation counting the number of neurons it contains. We follow the standard convention of the literature and denote by WR28\_ $n$  a network with  $64 \cdot n$  neurons obtained after average pooling the last  $64 \cdot n$  channels of the network. In our experiments we also analysed two narrow versions of the standard WR28\_1 which are not typically used in the literature. We named them WR28\_0.25 and WR28\_0.5 since they have 1/4 and 1/2 of the number of channels of WR28\_1.

**Reconstructing the wide representation from a smaller chunk.** To assess the predictive power of the chunk representations we search for the best linear map  $\mathbf{A}$ , of dimensions  $W \times w$ , able to minimise the squared difference  $(\mathbf{x}^{(W)} - \hat{\mathbf{x}}^{(W)})^2$  between the  $W$  activations of the full layer representation  $(\mathbf{x}^{(W)})$  and the activations predicted from a chunk of size  $w$ ,

$$\hat{\mathbf{x}}^{(W)} = \mathbf{A}\mathbf{x}^{(w)}. \quad (1)$$

This least squares problem is solved through a multi-output ridge regression [50] with regularisation set to  $10^{-8}$ , and we use the  $R^2$  value of the fit to measure the predictive power of a given chunk size. Such multi-output  $R^2$  value is computed as an average of the  $W$  single-output  $R^2$  values corresponding to the different coordinates, weighted by the variance of each coordinate. We further compute the covariance matrix  $C_{ij}$  (of dimensions  $W \times W$ ) of the residuals of this fit, and then obtain the correlation matrix as

$$\rho_{ij} = \frac{C_{ij}}{\sqrt{C_{ii}C_{jj} + 10^{-8}}}, \quad (2)$$

with a small regularisation in the denominator to avoid instabilities when the standard deviation of the residuals falls below machine precision. To quantify the independence of the chunk representations we take the average of the absolute values of the non-diagonal entries of the correlation matrix  $\rho_{ij}$ . For short we refer to this quantity as a ‘mean correlation’.

**Reproducibility** We provide code to reproduce our experiments and our analysis online at [https://anonymous.4open.science/r/representation\\_mitosis-EB80](https://anonymous.4open.science/r/representation_mitosis-EB80).

### 3 Results

**Random subsets of  $w$  neurons in the final representation of a wide network have similar predictive power to a network of width  $w$ .** We first compare the test error of a set of independently trained networks of increasing width with that of a single wide network where we chunked the feature space of the last layer. The top panels of Fig. 1 show the test accuracy of the classifiers as a function of the the number of activations of the last hidden layer of networks of increasing width (dashed lines) and of the chunk sizes of the wides architectures analysed (solid lines). The predictions in a chunked network are obtained selecting at random the number of neurons reported in the  $x$ -axis and averaging over 1000 repeated samples. These features are selected in the widest networks, corresponding to a fully-connected rectangular network with a total of 512 activations per layer (left), and a WR28\_8 whose last layer also has 512 activations (right). We do not fine tune the last layer weights after selecting a chunk. Remarkably, both in pMNIST and CIFAR10 the full and dashed lines follow approximately the same trend, indicating that the predictive power of a random chunk of features of a specific size is comparable to the predictive power of a network of the same width.

We find that the error decays to the ensemble average following a power law in the number of features with an exponent which is close to  $-1/2$  (dash-dotted line). For pMNIST, this trend is followed more closely if the network is optimised without regularisation, as in Ref. [24], while deviations are observed for chunk sizes of 16 and 32 if one uses batch normalization (see Methods). On the Wide-ResNets trained on CIFAR10 a significant deviation from this qualitative trend is observed only for chunk sizes of size 16 and 32.

**The intrinsic dimension of chunks of different sizes.** Figure 1 shows that the prediction accuracy of small chunks with  $w \leq 64$  on CIFAR10 decays faster than  $w^{-1/2}$ . A decay with rate  $1/2$  would suggest that adding neurons to the chunk adds additional measurements of features that are already used for prediction, with the increase in prediction accuracy coming from a statistically independent estimates of these features. The faster decay rate we observe implies that adding neurons in this regime gives new information to the chunk that is relevant for the classification task. A useful concept to quantify this notion is the *intrinsic dimension* [51] (ID). The ID indicates the minimum number of coordinates which are able to describe the data manifold without significant information loss, and it has been used extensively to investigate the properties of representations in deep neural networks [47, 51, 52].

In Fig. 2, we plot the ID of the final representation of networks of a given width, and for chunks taken from the representation of the widest networks. For pMNIST (orange curves), the ID profile is flat for all network and chunk sizes. For CIFAR10, we find that the ID of a chunk decreases compared to the ID of a full representation for sizes smaller than 128. This is the point at which we are losing information by taking a chunk instead of a full network of the same width. These results support the hypothesis that chunks can contain as much information about the data manifold as a full network of the same width, provided that they are large enough.

**The cross-over from random chunks to clones of the data manifold.** The ID of the widest representations gives a lower bound on the number of coordinates required to describe the data manifold, and hence on the neurons that a chunk needs in order to have the same classification accuracy as the whole representation. But how many neurons can we randomly sub-sample to obtain a chunk that has approximately the same predictive accuracy?

We investigate this question by verifying whether it is possible to reconstruct the representation of the last layer starting from a chunk of it. Since the last layer activations are used as inputs of a linear classifier, we reconstruct the value of the activations through a *linear* map from a chunk to the full layer representation. More precisely, we perform a regularised linear regression from the  $w$  activations of the chunk to the  $W$  activations of the full layer of the widest networks, as shown in Eq. (1).

The left column of Fig. 3 shows the  $R^2$  coefficient (blue) of the linear regression fit from a chunk to the widest representation as a function of the chunk size  $w$  for pMNIST and CIFAR10 (top and bottom, respectively). When  $w$  is really small, say below 10, the  $R^2$  coefficient grows linearly with  $w$ . In this region the number of features is of the order of magnitude of the intrinsic dimension of the data manifold ( $\sim 2$  for pMNIST,  $\sim 12$  for CIFAR10). Adding a random activation in the feature space will therefore increase substantially (almost linearly) the explained variance, namely  $R^2$ . When  $w$  becomes significantly larger than the ID, the network enters a “mitosis” phase, which is signalled

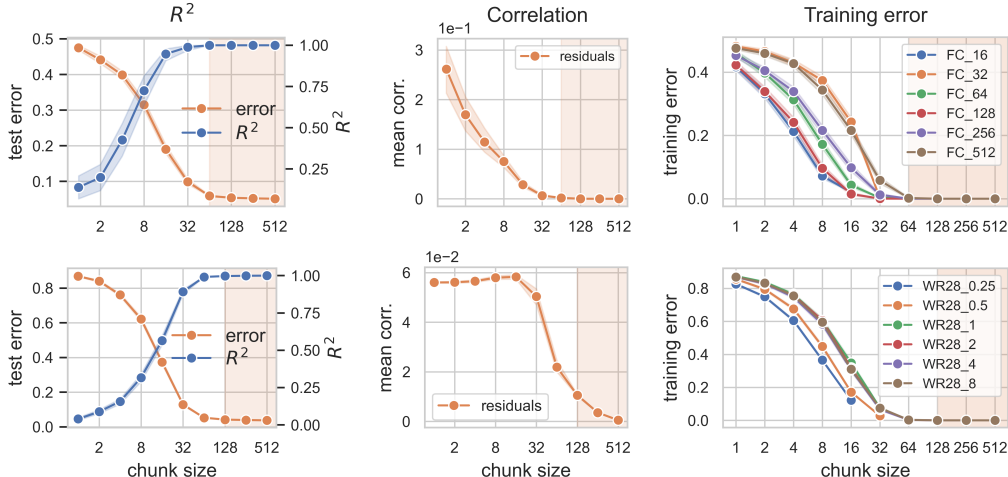


Figure 3: **Properties of chunks of different sizes.** Top and bottom rows correspond to pMNIST and CIFAR10 datasets respectively. Left column: The  $R^2$  value obtained in the fits (Eq. 1, blue) as well as the test error achieved by chunks of a given size (orange). Middle column: The ‘mean correlation’ of the residuals (Eq. 2, see Methods section for details). A low mean correlation indicates that the corresponding chunk representation is a copy of the full representation with the addition of a statistically independent error. Right column: Training error achieved by chunks of the full representations as a function of the chunk size. Different colours refer to networks with an increasingly wide last layer. Chunks of size greater or equal to 64 and 128 are able to achieve zero training error on pMNIST and CIFAR10 respectively.

by a striking event: the  $R^2$  becomes practically one. This happens around widths  $w \sim 64$  in pMNIST and  $w \sim 128$  in CIFAR10. These values correspond approximately to the width in which the test error (orange) starts scaling with the inverse square root of  $w$ , highlighted by vertical orange stripes. If the value of  $R^2$  were *exactly* one, the chunks would be exactly equivalent to the full representations, and averaging over the chunks would not improve the accuracy of the model<sup>2</sup>.

In the mitosis regime, the small residual difference between the chunk representation and the full representation can be modelled as statistically independent random noise. This is supported by the analysis shown in the two middle panels of Fig. 3, where we plot the mean absolute non-diagonal correlation of the residuals of the linear fit, a measure which indicates the level of correlation of the chunk representations with respect to the full representation (see Methods). Before the mitosis phase, the residuals are not only large, but also significantly correlated. Afterwards, the correlation drops basically to zero, consistently with the scaling law of the error in this phase. In practice, when the network becomes wide enough, any two chunks of equal size can be effectively considered as equivalent copies, or clones, of the same representation, differing only by a small and non-correlated noise.

The minimal size of a clone, namely a chunk with the same predictive accuracy as a full representation of the same width, can also be inferred from ability of chunks to fit the training set. Deep learning models typically have enough parameters to fit their training set with (close to) zero error [1, 2]. In the right column of Figure 3, we plot the training error of chunks of networks of various widths. Chunks of size greater or equal to 64 and 128 are able to achieve zero errors on pMNIST and CIFAR10, respectively. These are the chunk sizes at which the explained variance  $R^2$  approaches 1.

**The dynamics of mitosis.** Clones are formed in two stages, which occur at different times during training. The first phase begins as soon as training starts: the network gradually adjusts the chunk representations in order to produce maximally similar and independent copies of the data manifold. Such an effect can be clearly observed from the left panel of Fig. 4, which depict the correlation between chunk representations on the CIFAR10 dataset taken from the widest WR28\_8 as in Fig. 3,

<sup>2</sup>Indeed,  $R^2$  in this regime becomes simply much closer to one than for smaller  $w$ . Its value is 0.999 for  $w = 64$  in pMNIST and 0.997 for  $w = 128$  in CIFAR10



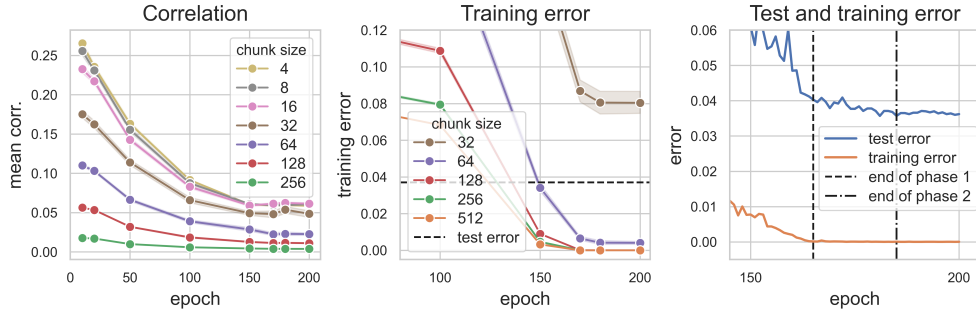


Figure 4: **Training dynamics.** Left: Mean correlation of chunks of the representations of the last layer of a WR28\_8 architecture trained on CIFAR10 as a function of the epoch number. Different curves correspond to different chunk sizes, as specified in the key. Middle: Training error as a function of the epoch for the full network (orange curve) and for chunks of different sizes (as specified in the key). Continuing the training of a wide network that has fitted the training set (at 160 epochs) allows improving significantly the training accuracy of the chunks. Right: Test and training error as a function of the epoch for the full network. Between epoch 160 and 180 the clones of the full network progressively achieve zero training error. In the same epochs, one observes a small improvement in the test error.

but now as a function of the training epoch. The figure reveals that the creation of clone representations of sizes greater than 64 starts immediately when training begins, as already at epoch 10 large chunk sizes have a small level of correlation. The correlation of the chunks continues to diminish gradually until epoch 160, after which further training does not bring any sizeable reduction in their correlation.

Remarkably, epoch 160 is also the epoch at which the full network achieves zero error on the training set, as shown in orange in the middle and right panels of Fig. 4. This event marks the end of the first phase, and the beginning of the second phase of the mitosis process. In the second phase, the full representation (orange) has already reached zero training error, but the training error of the clones keeps decreasing. For example, chunks of size 64 at epoch 150 have training errors comparable to the test error (dashed line of the middle panel). In the subsequent  $\sim 20$  epochs the training error of clones of size 128 and 256 reaches exactly zero, and the training error of chunks of size 64 reaches a plateau.

Importantly, both phases of mitosis improve the generalisation properties of the network. This can be seen in the right panel of Fig. 4, which reports training and test error of the network, with the two mitosis phases highlighted. The figure shows that both mitosis phases lead to a reduction in the test error, although the first phase leads by far to the greatest reduction, consistently with the fact that the greatest improvements in accuracy typically arise during the first epochs of training.

The mitosis process can be considered finished around epoch 180, when all the clones have reached zero error on the training set. After epoch 180 we also observe that the test error stops improving.

**Wide networks or deep ensemble averages?** We have shown that the last layer of a wide DNN can be viewed as an ensemble of statistical independent models of the data manifold which emerge autonomously during training. A natural question is then whether it is possible to tackle the learning problem using a *deep ensemble* [37, 38] of statistically independent models, each with a width corresponding to that of the clones. We find that the two procedures, training a single wide DNN and an ensemble of smaller DNNs, are indeed equivalent in terms of classification accuracy for the pMNIST dataset. Indeed in this case, as also shown in [24], averaging over a sufficiently large number of models leads always to the same asymptotic accuracy, almost independently on the width (see Fig. 5, left panel). The situation is very different for the CIFAR10 dataset, where the asymptotic accuracy of an ensemble average significantly increases with the width of the last layer (see Fig. 5, right panel). This result, which is consistent with the decreasing trend of the the ensemble loss as a function of the networks size observed in Lobacheva et al. [53], also shows a limit of the performance of a naive model combination [54].

As a consequence, to build a maximally accurate model on this dataset it is more convenient to train a single very wide DNN (for example a WR28\_8 architecture) rather than training many smaller DNNs

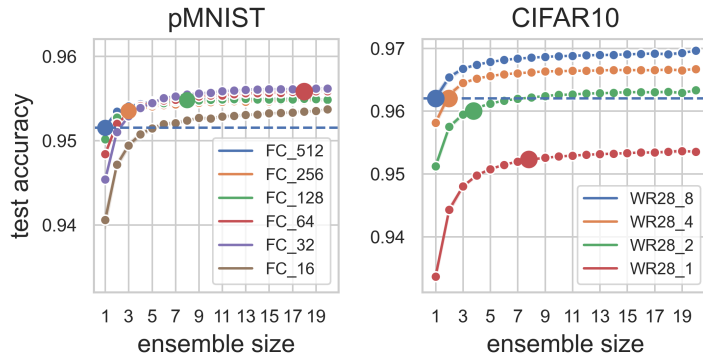


Figure 5: **Test accuracy of ensembles of networks.** Left and right panels correspond pMNIST and CIFAR10 datasets respectively. The test accuracy is plotted as a function of the size of the ensemble used to make the prediction. The different curves correspond to different architectures of the networks, as specified in the keys. The circles correspond to ensembles with the same memory consumption. The blue point corresponds to a single model, trained using the largest architecture (FC\_512 for pMNIST and WR28\_8 for CIFAR10).

(for example 8 statistically independent WR28\_1 architectures). This situation is even exacerbated when comparing the training accuracy conditioned on a fixed computational budget. In practice, for convolutional networks the memory footprint is dominated by the number of activations [55] which scales linearly with the network width  $w$ , rather than the number of parameters which instead scales quadratically with  $w$ . The large circles in Fig. 5 show the ensemble sizes that occupy the same memory of a WR28\_8 during training. A single WR28\_8 has a test accuracy of  $\sim 0.962$ , while the 'memory equivalent' ensemble of WR28\_1 has an accuracy  $\sim 0.952$ , which is, for this architecture, very close to the asymptotic limit. This implies that a model built with the clones automatically developed in wide network has a higher accuracy than a deep ensemble based on architectures with a smaller width.

## 4 Discussion

This work is an attempt to shed more light on the apparently paradoxical observation that over-parameterisation boosts the performance of DNNs. This "paradox" is actually not a peculiarity of DNNs: if one trains a prediction model with  $n$  parameters using the same training set, but using statistically independent learning schedules, one can obtain, say,  $m$  models which, in suitable conditions, provide predictions of the same quantity with independent noise due to initialisation, SGD schedule, etc. If one estimates the target quantity by an ensemble average, the statistical error will (ideally) scale with  $m^{-1/2}$ , and therefore with  $N^{-1/2}$ , where  $N = nm$  is the total number of parameters of the combined model. This will happen even if  $N$  is much larger than the number of data.

What is less trivial is that a DNN is able to accomplish this scaling within a single model, in which all the parameters are optimised collectively via minimisation of a single loss function. Our work describes a possible mechanism at the basis of this phenomenon in the special case of a neural networks in which the last layer is very wide. We observe that if the layer is wide enough, random subsets of its neurons can be viewed as approximately independent representations of the same data manifold (or clones). The number of clones grows linearly with the width of the layer. This implies a scaling of the error with the width of the layer as  $w^{-1/2}$ , which is qualitatively consistent with our observations.

**The impact of network architecture.** The capability of a network to produce statistically independent clones in its last layer is architecture-dependent, since we find that  $w$  should be much larger than the intrinsic dimension of the data manifold. It is important to note that the total number of parameters of a DNN scales with  $w$  in a manner which, in general, depends on the architecture. This



implies that, if the mitosis mechanism we propose is correct, the scaling of the test error with  $N$  will in general be architecture-dependent. We note that the scaling we find for the fully-connected networks in Fig. 1 is consistent with that reported in Fig. 6-D of Geiger et al. [24]. In particular, the maximum width considered here ( $w \leq 512$ ) corresponds to a total number of parameters  $N \leq 10^6$  in their graph. In this range the accuracy in Fig. 6-D decays approximately with  $N^{-1/4}$ , corresponding to  $w^{-1/2}$ . Ref. [24] also reports a crossover to a decay of the error with  $N^{-1/2}$  for  $N > 10^6$ . This regime is predicted by an analytical calculation, and is relevant when misclassified data lay close to the decision boundary. We also verified that if  $N$  is varied changing the depth and keeping the width fixed the test accuracy does not change significantly, consistently with a scaling dominated by  $w$  rather than by  $N$ .

**The impact of training.** Even for wide enough architectures, clones appear only if the training schedule is appropriately chosen. In our examples, by stopping the training too early, for example when the training error is similar to the test error, the chunks of the last representation would not become entirely independent from one another, and therefore they could not be considered clones. In fact, we have seen that the separation of the clones is completed only when the test error on a model restricted to each clone becomes very small.

**Explicit and implicit ensembling in deep learning** The success of various deep learning architectures and techniques has been linked to some form of ensembling. The performance of ResNets [56] has been linked to an effective ensembling of shallower networks due to the residual connections [57]. The successful Dropout regularisation technique [58] samples from an exponential number of “thinned” networks during training to prevent co-adaptation of hidden units. While this can be seen as a form of ensembling, here we make the key observation that co-adaptation of hidden units in the form of clones occurs in the deep networks we train, and is crucial for their improving performance with width.

**Relation to theoretical results in the mean-field regime.** Our empirical results also agree with recent theoretical results that were obtained for two-layer neural networks [31–36]. Among several other results, these works characterise the optimal solutions of shallow networks with two layers of weights trained on synthetic datasets with some chosen features. In the limit of infinite training data, these optimal solutions correspond to networks where neurons in the hidden layer duplicate the key features of the data. This idea is illustrated most easily in the teacher-student setup, where inputs are random Gaussian vectors and labels are given by the output of a shallow network with fixed weights, called the “teacher”. In the over-parameterised case where the trained network, the “student” has more neurons than its teacher, several student neurons will make almost independent copies of a single teacher neuron and take an effective average over these estimates when computing their output. The error of the student then scales inversely with the number of clones in its hidden layer. These “denoising solutions” were found in the complementary limits of wide hidden layer [31–34] and wide input dimension [35, 36]. In both cases, the error of the neural network was shown to decay as  $w^{-1/2}$ , which is the same scaling we found experimentally for deep networks.

**Possible practical implications** These results, although experimental and system-specific, suggest plausible guidelines for improving the accuracy of DNN models in practice. According to our analysis, architectures with a wide representation close to the output can help to develop accurate models. In order to trigger the development of independent clones, training should be continued until the training error is extremely small. Moreover, we find that one can practically check if mitosis has happened by performing the analysis described in Fig. 3. Finally, our analysis suggests that training a single large wide network can provide a better performance than an ensemble-based approach with the same parameter and memory budget.

## Acknowledgements

We thank Stéphane d’Ascoli, Maria Refinetti and Guido Sanguinetti for helpful discussions.

## Broader Impact

Due to the theoretical nature of this paper, a broader societal impact of this work is not anticipated. In terms of scientific broader impact, we believe that better understanding of the behaviour and the performance of neural networks will eventually lead to improvement of the state-of-the-art systems as well as enhancements of their reliability, security and interpretability.

## References

- [1] C. Zhang, S. Bengio, M. Hardt, B. Recht, and O. Vinyals. Understanding deep learning requires rethinking generalization. In *ICLR*, 2017.
- [2] D. Arpit, S. Jastrzebski, M.S. Kanwal, T. Maharaj, A. Fischer, A. Courville, and Y. Bengio. A Closer Look at Memorization in Deep Networks. In *Proceedings of the 34th International Conference on Machine Learning*, 2017.
- [3] S. Geman, E. Bienenstock, and R. Doursat. Neural networks and the bias/variance dilemma. *Neural computation*, 4(1):1–58, 1992.
- [4] B. Neyshabur, R. Tomioka, and N. Srebro. In search of the real inductive bias: On the role of implicit regularization in deep learning. In *ICLR*, 2015.
- [5] S Spigler, M Geiger, S d’Ascoli, L Sagun, G Biroli, and M Wyart. A jamming transition from under-to over-parametrization affects generalization in deep learning. *Journal of Physics A: Mathematical and Theoretical*, 52(47):474001, 2019.
- [6] P. Nakkiran, G. Kaplun, T. Bansal, Y. amd Yang, B. Barak, and I. Sutskever. Deep double descent: Where bigger models and more data hurt. arXiv:1912.02292, 2019.
- [7] S. Gunasekar, J. Lee, D. Soudry, and N. Srebro. Characterizing implicit bias in terms of optimization geometry. In *International Conference on Machine Learning*, pages 1832–1841. PMLR, 2018.
- [8] S. Gunasekar, J. Lee, D. Soudry, and N. Srebro. Implicit bias of gradient descent on linear convolutional networks. *arXiv preprint arXiv:1806.00468*, 2018.
- [9] D. Soudry, E. Hoffer, and N. Srebro. The implicit bias of gradient descent on separable data. In *International Conference on Learning Representations*, 2018.
- [10] Z. Ji and M. Telgarsky. The implicit bias of gradient descent on nonseparable data. In *Conference on Learning Theory*, pages 1772–1798. PMLR, 2019.
- [11] S. Arora, N. Cohen, W. Hu, and Y. Luo. Implicit regularization in deep matrix factorization. In H. Wallach, H. Larochelle, A. Beygelzimer, F. d’Alché-Buc, E. Fox, and R. Garnett, editors, *Advances in Neural Information Processing Systems*, volume 32. Curran Associates, Inc., 2019.
- [12] L. Chizat and F. Bach. Implicit bias of gradient descent for wide two-layer neural networks trained with the logistic loss. In *Conference on Learning Theory*, pages 1305–1338. PMLR, 2020.
- [13] H. S. Seung, H. Sompolinsky, and N. Tishby. Statistical mechanics of learning from examples. *Physical Review A*, 45(8):6056–6091, 1992.
- [14] A. Engel and C. Van den Broeck. *Statistical Mechanics of Learning*. Cambridge University Press, 2001.
- [15] B. Aubin, A. Maillard, J. Barbier, F. Krzakala, N. Macris, and L. Zdeborová. The committee machine: Computational to statistical gaps in learning a two-layers neural network. In *Advances in Neural Information Processing Systems 31*, pages 3227–3238, 2018.
- [16] M.S. Advani, A.M. Saxe, and H. Sompolinsky. High-dimensional dynamics of generalization error in neural networks. *Neural Networks*, 132:428 – 446, 2020.

- [17] B. Neal, S. Mittal, A. Baratin, V. Tantia, M. Scicluna, S. Lacoste-Julien, and I. Mitliagkas. A modern take on the bias-variance tradeoff in neural networks. *arXiv preprint arXiv:1810.08591*, 2018.
- [18] S. Mei and A. Montanari. The generalization error of random features regression: Precise asymptotics and double descent curve. *arXiv:1908.05355*, 2019.
- [19] M. Belkin, D. Hsu, S. Ma, and S. Mandal. Reconciling modern machine-learning practice and the classical bias–variance trade-off. *Proceedings of the National Academy of Sciences*, 116(32):15849–15854, 2019.
- [20] Trevor Hastie, Andrea Montanari, Saharon Rosset, and Ryan J Tibshirani. Surprises in high-dimensional ridgeless least squares interpolation. *arXiv preprint arXiv:1903.08560*, 2019.
- [21] S. d’Ascoli, M. Refinetti, G. Biroli, and F. Krzakala. Double trouble in double descent : Bias and variance(s) in the lazy regime. In *ICML*, 2020.
- [22] B. Adlam and J. Pennington. Understanding double descent requires a fine-grained bias-variance decomposition. In H. Larochelle, M. Ranzato, R. Hadsell, M. F. Balcan, and H. Lin, editors, *Advances in Neural Information Processing Systems*, volume 33, pages 11022–11032. Curran Associates, Inc., 2020.
- [23] Licong Lin and Edgar Dobriban. What causes the test error? going beyond bias-variance via anova. *arXiv preprint arXiv:2010.05170*, 2020.
- [24] Mario Geiger, Arthur Jacot, Stefano Spigler, Franck Gabriel, Levent Sagun, Stéphane d’Ascoli, Giulio Biroli, Clément Hongler, and Matthieu Wyart. Scaling description of generalization with number of parameters in deep learning. *Journal of Statistical Mechanics: Theory and Experiment*, 2020(2):023401, 2020.
- [25] P.L. Bartlett, P.M. Long, G. Lugosi, and A. Tsigler. Benign overfitting in linear regression. *Proceedings of the National Academy of Sciences*, 117(48):30063–30070, 2020.
- [26] S. Liu, D. Papailiopoulos, and D. Achlioptas. Bad global minima exist and sgd can reach them. In H. Larochelle, M. Ranzato, R. Hadsell, M. F. Balcan, and H. Lin, editors, *Advances in Neural Information Processing Systems*, volume 33, pages 8543–8552. Curran Associates, Inc., 2020.
- [27] B. Alberts, D. Bray, K. Hopkin, A.D. Johnson, J. Lewis, M. Raff, K. Roberts, and P. Walter. *Essential cell biology*. Garland Science, 2015.
- [28] S. Zagoruyko and N. Komodakis. Wide residual networks. *arXiv preprint arXiv:1605.07146*, 2016.
- [29] Y. LeCun and C. Cortes. The MNIST database of handwritten digits, 1998.
- [30] A. Krizhevsky, G. Hinton, et al. Learning multiple layers of features from tiny images. <https://www.cs.toronto.edu/~kriz/learning-features-2009-TR.pdf>, 2009.
- [31] S. Mei, A. Montanari, and P. Nguyen. A mean field view of the landscape of two-layer neural networks. *Proceedings of the National Academy of Sciences*, 115(33):E7665–E7671, 2018.
- [32] G.M. Rotskoff and E. Vanden-Eijnden. Parameters as interacting particles: long time convergence and asymptotic error scaling of neural networks. In *Advances in Neural Information Processing Systems 31*, pages 7146–7155, 2018.
- [33] L. Chizat and F. Bach. On the global convergence of gradient descent for over-parameterized models using optimal transport. In *Advances in Neural Information Processing Systems 31*, pages 3040–3050, 2018.
- [34] J. Sirignano and K. Spiliopoulos. Mean field analysis of neural networks: A central limit theorem. *Stochastic Processes and their Applications*, 2019.
- [35] S. Goldt, M.S. Advani, A.M. Saxe, F. Krzakala, and L. Zdeborová. Dynamics of stochastic gradient descent for two-layer neural networks in the teacher-student setup. In *Advances in Neural Information Processing Systems 32*, 2019.

- [36] M. Refinetti, S. Goldt, F. Krzakala, and L. Zdeborová. Classifying high-dimensional gaussian mixtures: Where kernel methods fail and neural networks succeed. In *ICML*, 2021.
- [37] T.G. Dietterich. Ensemble methods in machine learning. In *International workshop on multiple classifier systems*, pages 1–15. Springer, 2000.
- [38] B. Lakshminarayanan, A. Pritzel, and C. Blundell. Simple and scalable predictive uncertainty estimation using deep ensembles. In I. Guyon, U. V. Luxburg, S. Bengio, H. Wallach, R. Fergus, S. Vishwanathan, and R. Garnett, editors, *Advances in Neural Information Processing Systems*, volume 30. Curran Associates, Inc., 2017.
- [39] E. Littwin, B. Myara, S. Sabah, J. Susskind, S. Zhai, and O. Golan. Collegial ensembles. In H. Larochelle, M. Ranzato, R. Hadsell, M. F. Balcan, and H. Lin, editors, *Advances in Neural Information Processing Systems*, volume 33, pages 18738–18748. Curran Associates, Inc., 2020.
- [40] A. Jacot, F. Gabriel, and C. Hongler. Neural tangent kernel: Convergence and generalization in neural networks. In *Advances in Neural Information Processing Systems 32*, pages 8571–8580, 2018.
- [41] L. Chizat, E. Oyallon, and F. Bach. On lazy training in differentiable programming. In *Advances in Neural Information Processing Systems*, pages 2937–2947, 2019.
- [42] J. Hestness, S. Narang, N. Ardalani, G. Diamos, H. Jun, H. Kianinejad, M. Patwary, M. Ali, Y. Yang, and Y. Zhou. Deep learning scaling is predictable, empirically. *arXiv preprint arXiv:1712.00409*, 2017.
- [43] J.S. Rosenfeld, A. Rosenfeld, Y. Belinkov, and N. Shavit. A constructive prediction of the generalization error across scales. In *International Conference on Learning Representations*, 2020.
- [44] J. Kaplan, S. McCandlish, T. Henighan, T.B. Brown, B. Chess, R. Child, S. Gray, A. Radford, J. Wu, and D. Amodei. Scaling laws for neural language models. *arXiv preprint arXiv:2001.08361*, 2020.
- [45] T. Henighan, J. Kaplan, M. Katz, M. Chen, C. Hesse, J. Jackson, H. Jun, T.B. Brown, P. Dhariwal, S. Gray, et al. Scaling laws for autoregressive generative modeling. *arXiv preprint arXiv:2010.14701*, 2020.
- [46] Y. Bahri, E. Dyer, J. Kaplan, J. Lee, and U. Sharma. Explaining neural scaling laws. *arXiv preprint arXiv:2102.06701*, 2021.
- [47] U. Sharma and J. Kaplan. A neural scaling law from the dimension of the data manifold. *arXiv preprint arXiv:2004.10802*, 2020.
- [48] Ilya Loshchilov and Frank Hutter. Sgdr: Stochastic gradient descent with warm restarts. *arXiv preprint arXiv:1608.03983*, 2016.
- [49] Ekin D Cubuk, Barret Zoph, Jonathon Shlens, and Quoc V Le. Randaugment: Practical automated data augmentation with a reduced search space. In *Proceedings of the IEEE/CVF Conference on Computer Vision and Pattern Recognition Workshops*, pages 702–703, 2020.
- [50] Trevor Hastie, Robert Tibshirani, and Jerome Friedman. *The Elements of Statistical Learning*. Springer Series in Statistics. Springer New York Inc., New York, NY, USA, 2001.
- [51] Alessio Ansuini, Alessandro Laio, Jakob H Macke, and Davide Zoccolan. Intrinsic dimension of data representations in deep neural networks. In *Advances in Neural Information Processing Systems*, pages 6109–6119, 2019.
- [52] D. Doimo, A. Glielmo, A. Ansuini, and A. Laio. Hierarchical nucleation in deep neural networks. In H. Larochelle, M. Ranzato, R. Hadsell, M. F. Balcan, and H. Lin, editors, *Advances in Neural Information Processing Systems*, volume 33, pages 7526–7536. Curran Associates, Inc., 2020.

- [53] E. Lobacheva, N. Chirkova, M. Kodryan, and D.P. Vetrov. On power laws in deep ensembles. In H. Larochelle, M. Ranzato, R. Hadsell, M. F. Balcan, and H. Lin, editors, *Advances in Neural Information Processing Systems*, volume 33, pages 2375–2385. Curran Associates, Inc., 2020.
- [54] Florian Wenzel, Kevin Roth, Bastiaan S Veeling, Jakub Świątkowski, Linh Tran, Stephan Mandt, Jasper Snoek, Tim Salimans, Rodolphe Jenatton, and Sebastian Nowozin. How good is the bayes posterior in deep neural networks really? *arXiv preprint arXiv:2002.02405*, 2020.
- [55] I. Bello, W. Fedus, X. Du, E.D. Cubuk, A. Srinivas, T-Y. Lin, J. Shlens, and B. Zoph. Revisiting resnets: Improved training and scaling strategies. *arXiv preprint arXiv:2103.07579*, 2021.
- [56] K. He, X. Zhang, S. Ren, and J. Sun. Deep residual learning for image recognition. In *Proceedings of the IEEE conference on computer vision and pattern recognition*, pages 770–778, 2016.
- [57] Andreas Veit, Michael J Wilber, and Serge Belongie. Residual networks behave like ensembles of relatively shallow networks. In D. Lee, M. Sugiyama, U. Luxburg, I. Guyon, and R. Garnett, editors, *Advances in Neural Information Processing Systems*, volume 29. Curran Associates, Inc., 2016.
- [58] N. Srivastava, G. Hinton, A. Krizhevsky, I. Sutskever, and R. Salakhutdinov. Dropout: a simple way to prevent neural networks from overfitting. *The journal of machine learning research*, 15(1):1929–1958, 2014.

## Checklist

1. For all authors...
  - (a) Do the main claims made in the abstract and introduction accurately reflect the paper’s contributions and scope? [Yes]
  - (b) Did you describe the limitations of your work? [Yes]
  - (c) Did you discuss any potential negative societal impacts of your work? [Yes] Please consider the “Broader impact” section of our paper.
  - (d) Have you read the ethics review guidelines and ensured that your paper conforms to them? [Yes]
2. If you are including theoretical results...
  - (a) Did you state the full set of assumptions of all theoretical results? [N/A]
  - (b) Did you include complete proofs of all theoretical results? [N/A]
3. If you ran experiments...
  - (a) Did you include the code, data, and instructions needed to reproduce the main experimental results (either in the supplemental material or as a URL)? [Yes] We provide code to reproduce all our experiments and figures at [https://anonymous.4open.science/r/representation\\_mitosis-EB80](https://anonymous.4open.science/r/representation_mitosis-EB80).
  - (b) Did you specify all the training details (e.g., data splits, hyperparameters, how they were chosen)? [Yes] See Methods section.
  - (c) Did you report error bars (e.g., with respect to the random seed after running experiments multiple times)? [Yes]
  - (d) Did you include the total amount of compute and the type of resources used (e.g., type of GPUs, internal cluster, or cloud provider)? [Yes] We ran all our experiments on a single GPU GeForce GTX TITAN X.
4. If you are using existing assets (e.g., code, data, models) or curating/releasing new assets...
  - (a) If your work uses existing assets, did you cite the creators? [Yes] We used the standard MNIST [29] and CIFAR10 datasets [30]
  - (b) Did you mention the license of the assets? [N/A]
  - (c) Did you include any new assets either in the supplemental material or as a URL? [N/A]

- (d) Did you discuss whether and how consent was obtained from people whose data you're using/curating? [N/A]
  - (e) Did you discuss whether the data you are using/curating contains personally identifiable information or offensive content? [N/A]
5. If you used crowdsourcing or conducted research with human subjects...
- (a) Did you include the full text of instructions given to participants and screenshots, if applicable? [N/A]
  - (b) Did you describe any potential participant risks, with links to Institutional Review Board (IRB) approvals, if applicable? [N/A]
  - (c) Did you include the estimated hourly wage paid to participants and the total amount spent on participant compensation? [N/A]